Physics

Physics Research Publications

Purdue University *Year* 2006

Isotopic-mass dependence of the A, B, and C excitonic band gaps in ZnO at low temperatures

S. Tsoi* X. Lu† A. K. Ramdas‡

H. Alawadhi** M. Grimsditch††

M. Cardona‡‡ R. Lauck§

*

†

‡

**

††

‡‡

§

Isotopic-mass dependence of the A, B, and C excitonic band gaps in ZnO at low temperatures

S. Tsoi,* X. Lu, and A. K. Ramdas
Department of Physics, Purdue University, West Lafayette, Indiana 47907, USA

H. Alawadhi
Department of Basic Sciences, University of Sharjah, United Arab Emirates

M. Grimsditch
Argonne National Laboratory, Argonne, Illinois 60439, USA

M. Cardona and R. Lauck
Max-Planck-Institut für Festkörperforschung, Heisenbergstrasse 1, 70569 Stuttgart, Germany
(Received 4 May 2006; revised manuscript received 21 July 2006; published 4 October 2006)

Low temperature wavelength-modulated reflectivity measurements of isotopically engineered ZnO samples have yielded the dependence of their A, B, and C excitonic band gaps on the isotopic masses of Zn and O. The observed dependence is analyzed in terms of the band gap renormalization by zero-point vibrations via electron-phonon interaction and the volume dependence on isotopic mass. A simplified, two-oscillator model, employed in the analysis, yields zero-point renormalizations of the band gaps, -154 ± 14 meV (A), -145 ± 12 meV (B), and -169 ± 14 meV (C), for ZnO with natural isotopic composition.

DOI: 10.1103/PhysRevB.74.165203 PACS number(s): 78.55.Et, 63.20.Kr, 78.40.Fy

I. INTRODUCTION

With access to monoisotopic as well as isotopically enriched semiconductors, it has recently become possible to explore experimentally the dependence of their physical properties on the isotopic composition.[1,2] The dramatic increase in the thermal conductivity of diamond upon the elimination of the isotopic disorder involving the ^{13}C and ^{12}C isotopes[3,4] and the influence of isotopic composition on lattice dynamics[5] are two illustrative examples of novel physical phenomena which have come to light, thanks to the advent of isotopically engineered crystals.

In the context of isotope-related effects, one must underscore the fascinating renormalization of the band gaps observed in isotopically engineered semiconductors. The experiments on isotopically enriched elemental diamond,[6] Ge,[7–9] and Si (Ref. 10–12) have yielded with great precision both the bare band gaps for the *static* lattice and the corresponding renormalizations by zero-point vibrations through electron-phonon interaction and volume change associated with anharmonicity. These data provide invaluable information for band structure calculations and the theory of electron-phonon interaction. We note that a cogent interpretation of these experimental investigations has been possible because of the simplicity of the theoretical formulation for the isotopic mass dependence of the band gaps in elemental semiconductors.

In addition to those on elemental semiconductors, experimental studies of the isotopic effects on the electronic band gaps have been carried out in a number of III-V, II-VI, and I-VII compound semiconductors.[13] Isotope related phenomena become considerably richer as one proceeds from the elemental to compound semiconductors,[14–16] since the mass of each constituent element can affect the band gap and other physical properties differently. However, the analysis of the isotopic results in the compound semiconductors is more complicated in comparison to that in the elemental semiconductors.

In the context of phonon renormalization effects, ZnO is a compound semiconductor most suitable for exploring isotopic mass effects due to its light anion (O) and the heavier cation (Zn). In addition, its fundamental gap is direct; its wurtzite structure, coupled with the crystal field and spin-orbit splittings, produces three spectroscopically fully resolved direct excitons; and isotopically controlled ZnO specimens have been fabricated recently.

The isotopic dependence of the band gaps of ZnO was previously investigated by Kreingol'd and Kulinkin[17] using wavelength-modulated reflectivity for two samples with natural isotopic composition of O but different Zn isotopes and two samples with natural isotopic composition of Zn but different isotopic compositions of O. Recently, Manjón *et al.*[18] reported isotopic and temperature effects on the A excitonic band gap accessible in photoluminescence (PL). In the present investigation, we have exploited the modulated reflectivity technique to observe *all* the three excitonic signatures in ZnO samples with a significantly expanded range of isotopic compositions. We present in this paper the comprehensive data thus obtained as well as their theoretical analysis.

II. EXPERIMENT

The wurtzite ZnO single crystals studied in the present investigation were grown by chemical vapor transport after sublimation and oxidation of zinc (99.9995%) in a silica ampoule using ammonium chloride as a transport agent. Table I shows their nominal isotopic composition.[35] Our isotopically engineered samples have irregular shapes and their dimensions do not exceed 2 mm. The sample with natural isotopic content has a prismatic shape with a hexagonal base, its *c*

TABLE I. Isotopic composition of ZnO samples investigated in the present study.

$^{64}Zn^{16}O$
$^{nat}Zn^{nat}O$
$^{68}Zn^{16}O$
$^{nat}Zn^{16}O_{0.5}{}^{18}O_{0.5}$
$^{68}Zn^{16}O_{0.5}{}^{18}O_{0.5}$
$^{64}Zn^{18}O$
$^{nat}Zn^{18}O$
$^{68}Zn^{18}O$

axis being normal to it. All the samples belong to the same batches as those investigated in Ref. 19.

For the specimen with natural isotopic composition, unpolarized measurements were performed on the flat surfaces containing the *c* axis. Radiation from a Xe-arc lamp was passed through a monochromator, focused on the sample and retroreflected for detection with a Si-photodiode. Modulated reflectivity was obtained using either electro-, photo-, or wavelength-modulation in conjunction with phase-sensitive lock-in amplification. The details of the modulation techniques can be found elsewhere.[20]

The small size of the isotopically controlled samples resulted in low power of the reflected light, necessitating the use of a photomultiplier (PMT) as a detector. In order to reduce the amount of stray light detected by the PMT, it was directly coupled to the exit slit of a SPEX (model 1870) monochromator, and the sample, mounted in a variable temperature liquid helium cryostat, was placed in front of the entrance slit. Broadband radiation from the Xe-arc lamp was directly focused on the sample without passing through the monochromator. Small facets, produced during the growth, were identified in the samples under a magnifying glass and used for retroreflection. The incident radiation was linearly polarized with a Nicol prism.

III. THEORETICAL BACKGROUND

The variation in the band gap (E_G) of a crystal with isotopic mass (M) at fixed temperature (T) and pressure (P) can be expressed as

$$\left(\frac{\partial E_G}{\partial M}\right)_{T,P} = \left(\frac{\partial E_G}{\partial M}\right)_{T,V} + \frac{D}{V}\left(\frac{\partial V}{\partial M}\right)_{T,P}, \tag{1}$$

where $D=-B(\partial E_G/\partial P)_{T,M}$ is the deformation potential for hydrostatic strain and B is the bulk modulus. The first term on the right-hand side of Eq. (1) results from the electron-phonon interaction whereas the second is due to change in volume with isotopic mass.

At fixed T and P, the frequencies of the lattice vibrations and, therefore their amplitudes, are determined by M, the average isotopic mass over the whole crystal. Consequently, the electron-phonon interaction, treated as perturbation, leads to an M-dependent renormalization of the band gap of a *static* lattice. In addition, lattice vibrations coupled with anharmonicity of an interatomic potential result in an M-dependent volume different from that of the static lattice, which, in turn, also affects the band gap. Due to *zero-point vibrations*, such isotopic mass dependence is expected for the band gap even at absolute zero.

In the context of the dependence of any physical quantity on the isotopic mass, the static lattice can be conveniently represented by an *infinitely* massive isotope. Then, the renormalization of E_G^∞, the band gap of a static lattice, in a crystal with the average isotopic mass M on the basis of Eq. (1) is given by

$$E_G^\infty - E_G(T,P,M) = \int_M^\infty \left(\frac{\partial E_G}{\partial M'}\right)_{T,P} dM' = \int_M^\infty \left(\frac{\partial E_G}{\partial M'}\right)_{T,V} dM' + \int_M^\infty \frac{D}{V}\left(\frac{\partial V}{\partial M'}\right)_{T,P} dM'. \tag{2}$$

The renormalization by the electron-phonon interaction, i.e., the first term on the right-hand side of Eq. (2), is given by Eq. (3) of Ref. 14, i.e.,

$$\int_M^\infty \left(\frac{\partial E_G}{\partial M'}\right)_{T,V} dM' = \sum_{j,\mathbf{q}} \left(\frac{\partial E_G}{\partial n_{j,\mathbf{q}}}\right)\left(n_{j,\mathbf{q}} + \frac{1}{2}\right), \tag{3}$$

where the sum is taken over all phonon modes, characterized by wave vector $\mathbf{q}$ and the branch j, their population varying with temperature according to Bose-Einstein statistics. The renormalization due to the isotopic dependence of volume, i.e., the second term on the right-hand side of Eq. (2), can be evaluated as follows:

$$\int_M^\infty \frac{D}{V}\left(\frac{\partial V}{\partial M'}\right) dM' = -D \ln \frac{V(T,P,M)}{V_0}, \tag{4}$$

where V_0 is the volume of the static lattice and $V(T,P,M)$ that of a crystal with the average isotopic mass M. An analytical expression for $V(T,P,M)$ is given in Eq. (2.3) of Ref. 21, i.e.,

$$V(T,P,M) = V_0 + \frac{1}{B}\sum_{j,\mathbf{q}} \hbar\,\Omega_j(\mathbf{q})\,\gamma_j(\mathbf{q})\left(n_{j,\mathbf{q}} + \frac{1}{2}\right), \tag{5}$$

where $\Omega_j(\mathbf{q})$ is the frequency of the phonon mode $j,\mathbf{q}$ and

$$\gamma_j(\mathbf{q}) = -\left.\frac{V_0}{\Omega_j(\mathbf{q})}\frac{\partial \Omega_j(\mathbf{q})}{\partial V}\right|_{V_0},$$

its mode Grüneisen parameter. Since under experimental conditions relevant to the present investigation the second term on the right-hand side of Eq. (5) is much smaller than the first term, Eq. (4) can be approximated by

$$\int_M^\infty \frac{D}{V}\left(\frac{\partial V}{\partial M'}\right) dM' \approx -\frac{D}{BV_0}\sum_{j,\mathbf{q}} \hbar\,\Omega_j(\mathbf{q})\,\gamma_j(\mathbf{q})\left(n_{j,\mathbf{q}} + \frac{1}{2}\right). \tag{6}$$

Although a calculation of the coefficients $(\partial E_G/\partial n_{j,\mathbf{q}})$ and the Grüneisen constants $\gamma_j(\mathbf{q})$ is possible,[22] provided one has good knowledge of the electron band structure and the lattice dynamics, a much simplified, *two-oscillator* model allows a

good physical description of the renormalization effects.[14,16,23] It must be pointed out, however, that at very low temperatures, the two-oscillator model cannot satisfactorily describe the temperature dependence of the band gap renormalization and the Debye model must be employed instead. Indeed, at low temperatures, the Debye model predicts a T^4 dependence of the band gap, which was recently proposed and demonstrated experimentally for Si.[24]

In the two-oscillator model, the lattice dynamics of the semiconductor is approximated by two harmonic oscillators, usually an average acoustic and an average optic mode. For binary compounds with a large difference in the masses of the anion and the cation, as in the case of ZnO, the amplitude of the acoustic mode is dominated by the heavy mass (Zn) and that of the optic mode by the light mass (O). Hence Eqs. (3) and (6) can be written as

$$\int_M^\infty \left(\frac{\partial E_G}{\partial M'}\right)_{T,V} dM' = \frac{p_{\mathrm{Zn}} A_{\mathrm{Zn}}}{\Omega_{\mathrm{Zn}} M_{\mathrm{Zn}}}\left(\frac{1}{\exp(\hbar\Omega_{\mathrm{Zn}}/k_B T)-1}+\frac{1}{2}\right) + \frac{p_{\mathrm{O}} A_{\mathrm{O}}}{\Omega_{\mathrm{O}} M_{\mathrm{O}}}\left(\frac{1}{\exp(\hbar\Omega_{\mathrm{O}}/k_B T)-1}+\frac{1}{2}\right), \tag{7}$$

and

$$\int_M^\infty \frac{D}{V}\left(\frac{\partial V}{\partial M'}\right) dM' = -\frac{p_{\mathrm{Zn}} D\hbar\,\Omega_{\mathrm{Zn}}\gamma_{\mathrm{Zn}}}{BV_0} \times\left(\frac{1}{\exp(\hbar\Omega_{\mathrm{Zn}}/k_B T)-1}+\frac{1}{2}\right) - \frac{p_{\mathrm{O}} D\hbar\,\Omega_{\mathrm{O}}\gamma_{\mathrm{O}}}{BV_0} \times\left(\frac{1}{\exp(\hbar\Omega_{\mathrm{O}}/k_B T)-1}+\frac{1}{2}\right). \tag{8}$$

Here Ω_{Zn} and Ω_{O} are the average frequencies of the Zn-dominated modes[36] and the optic, O-dominated modes, respectively; γ_{Zn}, γ_{O}, the corresponding average Grüneisen parameters; p_{Zn}, p_{O}, the degeneracies of the average optic and the average acoustic oscillators; M_{Zn} and M_{O} represent average isotopic masses of Zn and O; and A_{Zn} and A_{O}, parameters[14] describing the corresponding electron-phonon interactions. We note that upon the transition from Eq. (6) to Eq. (8), V_0 becomes the volume of the primitive cell. While it is doubly as large in wurtzite as in zinc blende, $p_{\mathrm{Zn}}=p_{\mathrm{O}}=6$ in wurtzite and $p_{\mathrm{Zn}}=p_{\mathrm{O}}=3$ in zinc blende.

Since Ω_{Zn} and Ω_{O} scale like the inverse of the square root of the corresponding mass and the Grüneisen constants are mass independent, it follows from Eqs. (7) and (8) that the isotopic mass dependence is most pronounced at low temperatures and tends to zero for $k_B T \gg \hbar\Omega_{\mathrm{Zn}}, \hbar\Omega_{\mathrm{O}}$. In this context, the present studies at liquid He temperatures correspond to the low temperature case.

Combining Eqs. (2), (7), and (8) for $T=0$ K, the zero-point renormalization of the band gap is described by

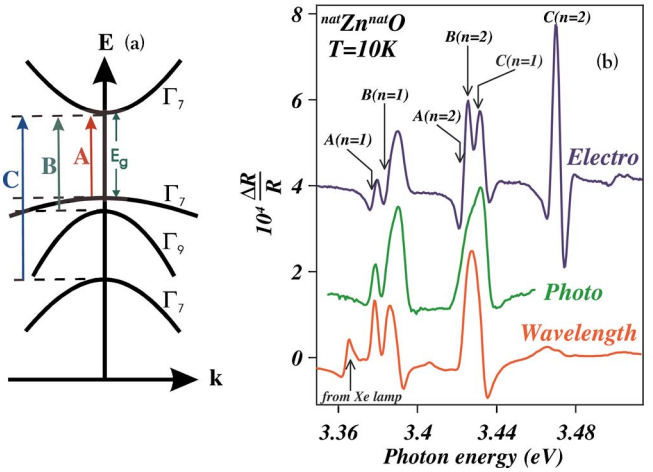

FIG. 1. (Color online) (a) Schematic representation of the conduction and valence bands of ZnO, showing their symmetries and associated A, B, and C band gaps. (b) Modulated reflectivity spectra of ZnO with constituents having natural isotopic composition, obtained with unpolarized light using electro-, photo-, and wavelength-modulation. The feature labeled "from Xe lamp" is due to the radiation from the source.

$$E_G(T=0, M_{\mathrm{Zn}}, M_{\mathrm{O}}) = E_G^\infty + \frac{C_{\mathrm{Zn}}}{M_{\mathrm{Zn}}^{1/2}} + \frac{C_{\mathrm{O}}}{M_{\mathrm{O}}^{1/2}}, \tag{9}$$

where

$$C = -\frac{pA}{2\Omega M^{1/2}} + \frac{pD\hbar\,\Omega\gamma M^{1/2}}{2BV_0}.$$

Thus the two-oscillator model provides a simple analytical expression for the dependence of the band gap on isotopic mass in the binary compound semiconductor under consideration, provided the cation and anion masses are significantly different.

IV. EXPERIMENTAL RESULTS AND DISCUSSION

Taking into account the crystal field and spin-orbit interactions[25] appropriate to the wurtzite structure, the valence band of ZnO near its Γ-point maximum is split into three doubly degenerate subbands, two of them belonging to the Γ_7 and the third to the Γ_9 symmetry of the C_{6v} point group of wurtzite. The conduction band minimum, also at the Γ-point, has Γ_7 symmetry. The polarization selection rules derived from group theory indicate that the $\Gamma_9 \rightarrow \Gamma_7$ transitions are allowed for polarization perpendicular to the c axis and the $\Gamma_7 \rightarrow \Gamma_7$ transitions for both parallel and perpendicular polarizations. Liang and Yoffe[26] observed in transmission experiments two strong transitions (A and B) for the perpendicular polarization and one (C) for the parallel, the order of the transitions with increasing energy being A, B, and C. In addition, the A line was observed as a weak transition in the parallel polarization and the C line in the perpendicular polarization. Based on these polarization features, they deduced the order of the valence band maxima with increasing energy to be Γ_7, Γ_9, and Γ_7 as shown in Fig. 1(a).

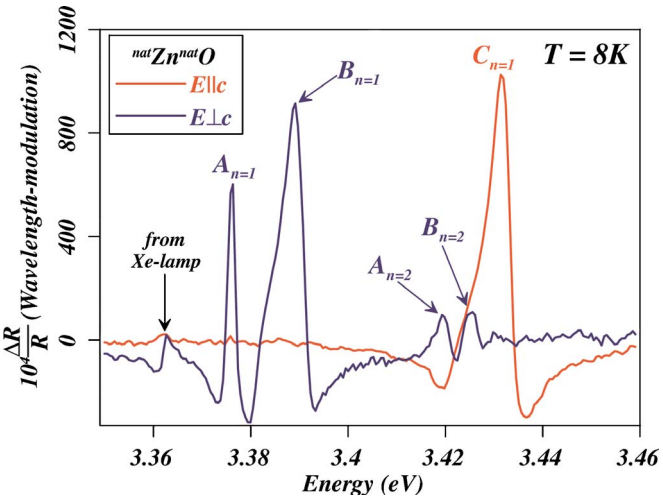

FIG. 2. (Color online) Wavelength-modulated reflectivity of $^{nat}Zn^{nat}O$ for light polarized parallel and perpendicular to the c axis.

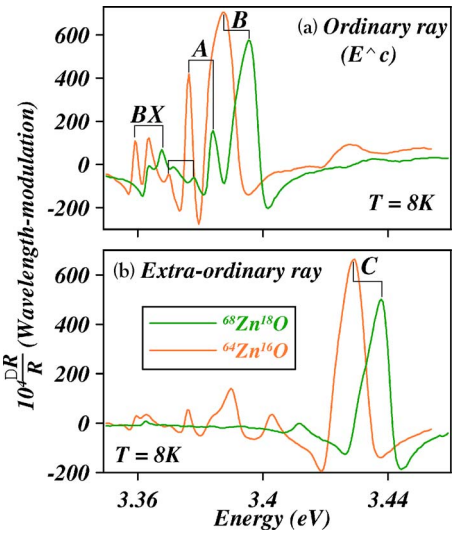

FIG. 3. (Color online) Wavelength-modulated reflectivity spectra of $^{64}Zn^{16}O$ and $^{68}Zn^{18}O$, recorded for the ordinary and extraordinary rays and $T=8$ K.

Figure 1(b) shows the modulated reflectivity spectra of ZnO with constituents having natural isotopic abundance, recorded with unpolarized light at $T=10$ K, using different modulation methods. The spectra display Lorentz-derivative-like signatures associated with the ground ($n=1$) and first excited ($n=2$) excitonic states of A, B, and C. Wavelength-modulated reflectivity spectra obtained with polarized light are displayed in Fig. 2. While the A and B features are observed for polarization perpendicular to the c axis, C is seen for parallel polarization. Although A and C are allowed for both polarizations, in our measurements A is not observed for the parallel polarization, nor is C for the perpendicular polarization. This is not surprising considering the weakness of the transitions for these polarizations, as reported in Ref. 26.

The isotopic shift of the A, B, and C excitonic band gaps at 8 K is displayed in Fig. 3 as an illustrative example. Features labeled *BX* are due to bound-exciton PL,[18] excited by the broadband radiation source. Since the isotopic samples investigated have irregular shapes, the incident light does not necessarily propagate perpendicular to the c axis, but rather at an arbitrary nonzero angle to it. Under these circumstances, the incident ordinary ray, with the polarization perpendicular to the c axis, can be chosen by rotating the linear polarizer until C disappears. The extraordinary ray obtained by further rotation of the polarizer by 90° may also have polarization perpendicular to the c axis in addition to the parallel one, thus explaining the appearance of A and B for the extraordinary ray in some of the samples.

The line shape of the observed wavelength-modulated reflectivity spectra of ZnO cannot be accounted for by the expressions[27] for Lorentzian excitonic resonance, but requires the polariton model.[28,29] In this model, the strong interaction of excitons with the electromagnetic field inside a semiconductor requires a description in which "the coupled exciton-radiation field" propagates as a combined mode called "polariton." Following Ref. 29, we consider the dispersion of the polariton

$$\frac{k^2c^2}{\omega^2} = \epsilon_\infty + \sum_{j=1}^{r} \frac{4\pi F_j \omega_j^2}{\omega_j^2 - \omega^2 + \hbar\,\omega_j k^2/M_j - i\omega\Gamma_j}, \tag{10}$$

where k and ω are the wave vector and angular frequency of the polariton, and F_j and ω_j the zero-frequency polarizability and frequency of the excitonic resonance labeled j, respectively. The center-of-mass masses M_j, i.e., the translational masses (the sum of electron and hole mass), determine the spatial dispersion[28] of the excitons and the exciton damping parameters Γ_j are assumed to be frequency independent. The summation in Eq. (10) is taken over r exciton resonances in the vicinity of ω and the background dielectric constant ϵ_∞ represents the sum over all other resonances, including electronic interband transitions which take place above the frequencies of the A, B, and C excitons.

In ZnO, the A and B resonances are separated by only 5 meV, whereas B and C are separated by 40 meV; thus for a polariton in the vicinity of A and B (Fig. 2) one needs to consider their contributions to Eq. (10) simultaneously, i.e., $r=2$. The resulting dispersion relation of Eq. (10) is cubic in k^2, implying three polariton modes with different k for a given ω. In contrast, a single isolated excitonic resonance C (Fig. 2) contributes to the polariton in its vicinity, resulting in two polariton modes according to Eq. (10). We note in addition that the polariton must have a nonzero electric field perpendicular to the c axis in order to couple to A and B and parallel to it to couple to C.

After solving Eq. (10) for $k_i^2(\omega)$, the polarization P_{ij}, associated with the polariton i and the excitonic resonance j, can be written as

$$P_{ij}(\omega) = \frac{E_i(\omega) F_j \omega_j^2}{\omega_j^2 - \omega^2 + \hbar\,\omega_j k_i^2(\omega)/M_j - i\omega\Gamma_j}, \quad i = 1, \ldots, r+1, \tag{11}$$

where $E_i(\omega)$ is the electric field of the polariton. The reflectivity at ω can now be obtained considering incident and

reflected electromagnetic waves with amplitudes $E_0(\omega)$ and $E_R(\omega)$, respectively, outside the semiconductor and $r+1$ polariton modes with amplitudes $E_i(\omega)$ inside. The usual Maxwell boundary conditions for the electric and magnetic field yield

$$E_0 + E_R = \sum_{i=1}^{r+1} E_i,$$

$$E_0 - E_R = \sum_{i=1}^{r+1} n_i E_i, \tag{12}$$

where $n_i = ck_i/\omega$ and the semiconductor is assumed to be in vacuum.

Equations (12) are not sufficient to uniquely determine E_0 and E_R. For this purpose Pekar introduced[30] the *additional boundary condition* (ABC) for the case of a single excitonic resonance, viz. the net polarization of the polaritons must disappear at the semiconductor boundary. Skettrup and Balslev[29] extended the additional boundary condition to multiple resonances by requiring the cancellation of the net polariton polarization at the surface, including all resonances:

$$\sum_{i=1}^{r+1} P_{ij}(\omega) = 0, \quad 1 \le j \le r. \tag{13}$$

A system of $r+2$ equations (12) and (13), with the polarizations P_{ij} expressed in terms of E_i by means of Eqs. (11), can be solved for E_R in terms of E_0, thus yielding the complex reflectance $r(\omega) = E_R(\omega)/E_0(\omega)$.

Hopfield and Thomas[28] pointed out that the exciton polarizations P_{ij} should disappear inside a surface layer of thickness l which they labeled as *dead* layer, rather than at the boundary of the semiconductor. The dead layer has been attributed to the finite size of the exciton in the semiconductor, characterized by its Bohr radius, which results in the electrostatic repulsion of the exciton from the surface layer. Consequently, one must consider reflection of the light from a double-layered surface, including interference[31] of the rays reflected from the two interfaces. The problem involves the incident (E_0) and reflected (E_R) electromagnetic waves outside the semiconductor, the incident (E_0') and reflected (E_R') electromagnetic waves inside the dead layer, characterized by the background dielectric constant ϵ_∞, and $r+1$ polariton modes in the rest of the semiconductor. The resultant complex reflectance is given by[31]

$$r(\omega) = \frac{r_{12} + r_{23} e^{i4\pi l/\lambda}}{1 + r_{12} r_{23} e^{i4\pi l/\lambda}}, \tag{14}$$

where $r_{12} = (1-\sqrt{\epsilon_\infty})/(1+\sqrt{\epsilon_\infty})$ is the reflectance from the vacuum-dead layer interface, r_{23} the reflectance from the dead layer-semiconductor interface, and λ the wavelength of the electromagnetic wave inside the dead layer.

Figures 4 and 5 show $(\partial R/\partial\lambda)$, the derivatives of the reflectivity, measured using wavelength modulation in different isotopic ZnO crystals and the corresponding fits obtained with the polariton model and the ABCs described above. For the purpose of finding the best fits, the polarizabilities F_j, the

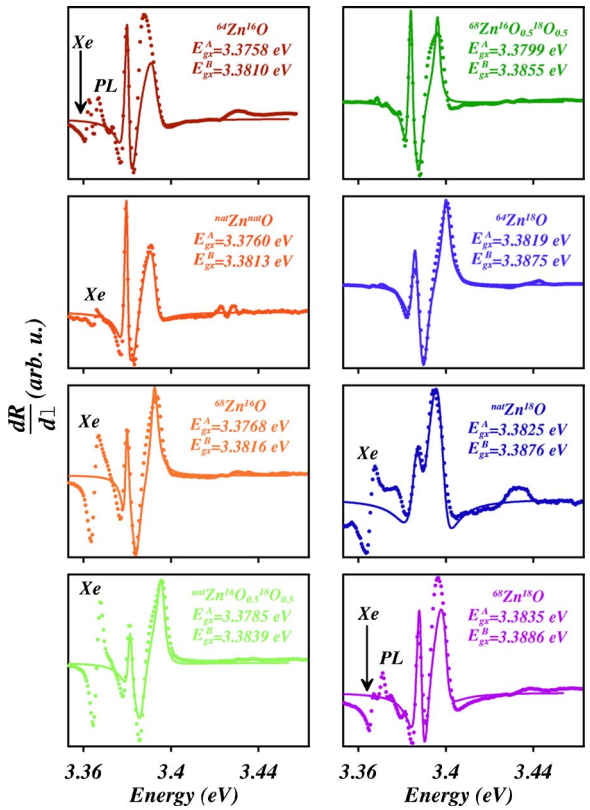

FIG. 4. (Color online) Derivative reflectivity spectra of isotopically controlled ZnO for the ordinary rays, obtained with wavelength modulation (dots), and corresponding fits (lines) obtained with the polariton model. The energies of the transverse A and B excitonic band gaps E_{gx}^A and E_{gx}^B are deduced from the fits. *PL* denotes bound-exciton photoluminescence excited by the broadband radiation from the source. Xe is a feature associated with the radiation from the xenon lamp.

damping parameters Γ_j, the background dielectric constant ϵ_∞, the thickness of the dead layer l, and the energies of the excitonic resonances $\hbar\omega_j$ are treated as fitting parameters. During the fitting procedure it was established that the exciton masses M_j did not significantly affect the line shape; they were fixed at $M_j = 1.8m_0$ (Ref. 29) (j=A,B,C), m_0 being the free electron mass. Table II shows the energies of excitonic resonances deduced from the fitting procedure.

Absent or weak features associated with the C polariton in Fig. 4 indicate that these spectra were obtained for the transverse polaritons, polarized perpendicular to the c axis. Thus the excitonic energies deduced in the fits represent transverse excitonic energies $\hbar\omega_A^T$ and $\hbar\omega_B^T$. In a similar fashion, the spectra with the absent or weak A and B features in Fig. 5 are attributed to transverse polariton polarized parallel to the c axis. In contrast, the rather distinct A and B polariton features seen in Fig. 5 for $^{64}Zn^{16}O$ are evidence of the polariton electric field having nonzero projections parallel and perpendicular to the c axis. This occurs when the polariton propagates at an arbitrary angle (i.e., other than 0° and 90°) to the c axis with the polarization in the plane containing the c axis and the propagation direction of the polariton. Under such circumstances, the polariton has a mixed, transverse-longitudinal character.[32] Since the line-shape analysis em-

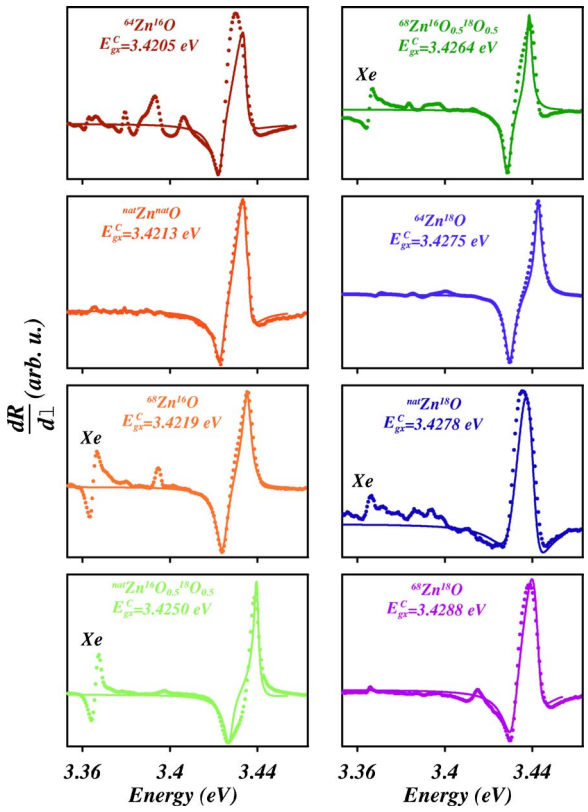

FIG. 5. (Color online) Same as in Fig. 4 for extraordinary rays. The energies of the transverse C excitonic band gaps E_{gx}^C are deduced from the fits. Xe is a feature associated with the radiation from the xenon lamp.

ployed in the present work is not valid for a mixed transverse-longitudinal polariton,[28] it was not possible to reliably determine the transverse excitonic energy $\hbar\omega_C^T$ for $^{64}Zn^{16}O$ from the recorded spectrum.

The longitudinal-transverse splittings of the excitons can be calculated (Table III) following Ref. 32 and using the parameters obtained from the fits. The splittings thus determined are comparable to the values measured in natural ZnO

TABLE II. Energies of the A, B, and C excitonic resonances determined for isotopically controlled ZnO samples from the fits to their wavelength-modulated reflectivity spectra using the polariton procedure described in the text. For additional parameters see Ref. 20.

	$\hbar\omega_A$ (eV)	$\hbar\omega_B$ (eV)	$\hbar\omega_C$ (eV)
$^{64}Zn^{16}O$	3.3758	3.381	
$^{nat}Zn^{nat}O$	3.3760	3.3813	3.4213
$^{68}Zn^{16}O$	3.3768	3.3816	3.4219
$^{nat}Zn^{16}O_{0.5}{}^{18}O_{0.5}$	3.3785	3.3839	3.4250
$^{68}Zn^{16}O_{0.5}{}^{18}O_{0.5}$	3.3799	3.3855	3.4264
$^{64}Zn^{18}O$	3.3819	3.3875	3.4275
$^{nat}Zn^{18}O$	3.3825	3.3876	3.4278
$^{68}Zn^{18}O$	3.3835	3.3883	3.4288

TABLE III. Longitudinal-transverse splittings of the A, B, and C excitons in ZnO, determined from the fitting parameters listed in Table II.

	$\hbar\omega_A^{LT}$ (meV)	$\hbar\omega_B^{LT}$ (meV)	$\hbar\omega_C^{LT}$ (meV)
$^{64}Zn^{16}O$	2.5	11.2	
$^{nat}Zn^{nat}O$	1.9	9.7	12.5
$^{68}Zn^{16}O$	1.9	8.7	11.5
$^{nat}Zn^{16}O_{0.5}{}^{18}O_{0.5}$	1.0	10.0	12.5
$^{68}Zn^{16}O_{0.5}{}^{18}O_{0.5}$	2.3	8.7	10.0
$^{64}Zn^{18}O$	2.3	10.5	13.0
$^{nat}Zn^{18}O$	2.9	9.8	11.0
$^{68}Zn^{18}O$	2.8	9.7	12.0

for the A and B excitons by Hopfield and Thomas in transmission[32] and for the C exciton by Lagois and Hümmer in reflection.[33] We note that they exhibit no significant dependence on isotopic mass, a fact that was also noticed for CdS.[13]

The low-temperature energies of the A, B, and C transverse excitonic band gaps, deduced from the fits, are plotted in Figs. 6–8 as a function of the total mass (in amu) of the ZnO molecular unit, i.e., $M_{Zn}+M_O$. Within the small range of available masses, the predicted isotopic dependence of Eq. (9) can be approximated by a linear dependence on the masses of Zn and O. The resulting linear fits, with the mass of either Zn or O fixed, are shown by solid lines, with the corresponding slopes given in meV/amu in parenthesis. The isotopic dependences of E_{gx}, obtained by taking into account the data for all the samples, are given in the rows $(\partial E_{gx}/\partial M_{Zn})_{T,P}$ and $(\partial E_{gx}/\partial M_O)_{T,P}$ of Table IV. They are in agreement with the values (0.37 ± 0.06) and (3.38 ± 0.38) meV/amu, respectively, measured for all three

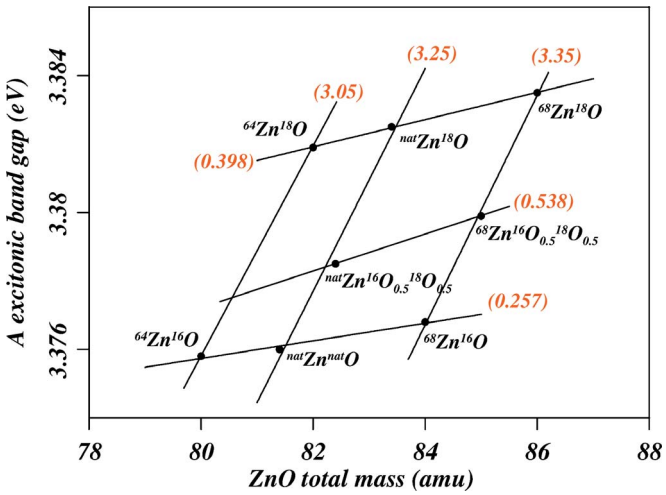

FIG. 6. (Color online) Dependence of the A excitonic band gap of ZnO on isotopic masses plotted as a function of the sum of the masses of Zn and O. The dots represent experimental data, the lines are linear fits, and the numbers in brackets give the slopes of the fits (in meV/amu).

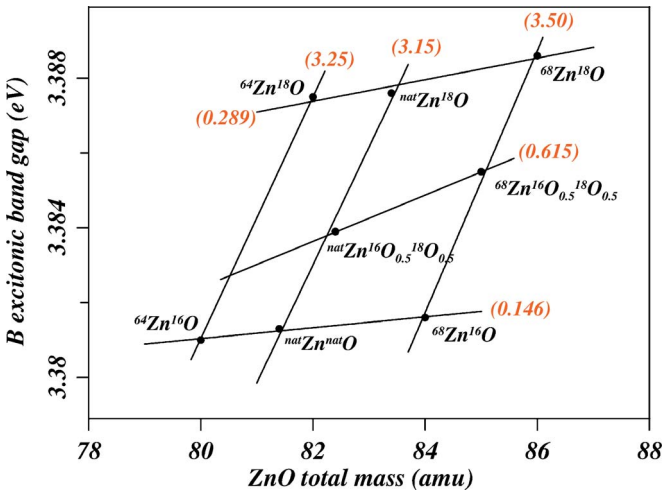

FIG. 7. (Color online) Isotopic mass dependence of the B excitonic band gap of ZnO plotted as in Fig. 6. The dots represent experimental data, the lines are linear fits, and the numbers in brackets give the slopes of the fits (in meV/amu).

band gaps by Kreingol'd and Kulinkin,[17] and with (0.41±0.05) and (3.22±0.10) meV/amu, respectively, measured by Manjón *et al.*[18] for the A excitonic gap.

The contributions $(D/V)(\partial V/\partial M)_{T,P}$ due to the volume dependence on isotopic mass can be easily estimated using Eq. (8) for $T=0$ K, assuming, for the sake of simplicity, the zinc-blende modification of ZnO (i.e., $p_{\mathrm{Zn}}=p_{\mathrm{O}}=3$)

$$\frac{1}{V}\left(\frac{\partial V}{\partial M_{\mathrm{Zn(O)}}}\right)_{T,P,M_{\mathrm{O(Zn)}}} = -\frac{3\hbar\,\Omega_{\mathrm{Zn(O)}}\gamma_{\mathrm{Zn(O)}}}{4BV_0M_{\mathrm{Zn(O)}}}. \qquad (15)$$

The average Grüneisen parameters as well as the average of the energies of acoustic and optical phonons can be estimated from Table VII of Ref. 34, i.e., $\gamma_{\mathrm{Zn}}\approx -0.9$, $\gamma_{\mathrm{O}}\approx 1.6$, $\hbar\Omega_{\mathrm{Zn}}\approx 20.1$ meV, and $\hbar\Omega_{\mathrm{O}}\approx 63.2$ meV. Using V_0 =24.65 Å (Ref. 3) and $B=160.8$ GPa,[34] appropriate for the cubic ZnO, and $M_{\mathrm{Zn}}=65.4$ amu, $M_{\mathrm{O}}=16$ amu, we obtain $(1/V)(\partial V/\partial M_{\mathrm{Zn}})_{T,P,M_{\mathrm{O}}}=8.4\times10^{-6}$ amu^{-1} and $(1/V)\times(\partial V/\partial M_{\mathrm{O}})_{T,P,M_{\mathrm{Zn}}}=-1.9\times10^{-4}$ amu^{-1}. Note that the derivative with respect to the oxygen mass is about half that obtained for diamond (4.5×10^{-4} amu^{-1}). We also notice that the derivative with respect to the Zn mass is much smaller and has the opposite sign. It would be interesting to measure these derivatives by x-ray diffraction and check whether they have opposite signs. The Grüneisen parameter γ_{Zn} has a small magnitude, a fact which results from a compensation of the various contributing acoustic branches. The average value can thus end up being either positive or negative if a fine mesh sampling over the Brillouin zone is made.

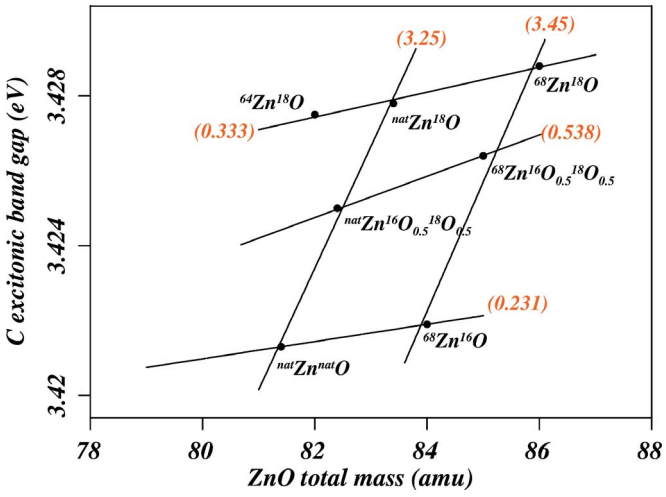

FIG. 8. (Color online) Isotopic mass dependence of the C excitonic band gap of ZnO plotted as in Fig. 6. The dots represent experimental data, the lines are linear fits, and the numbers in brackets give the slopes of the fits (in meV/amu).

Employing $D=-B(\partial E_{gx}/\partial P)_{T,M}$, together with $(\partial E^A_{gx}/\partial P)_{T,M}=23.6$ meV/GPa, $(\partial E^B_{gx}/\partial P)_{T,M}=24.4$ meV/GPa, and $(\partial E^C_{gx}/\partial P)_{T,M}=26.5$ meV/GPa,[25] we estimate the values of $(D/V)(\partial V/\partial M_{\mathrm{Zn}})_{T,P}$ and $(D/V)(\partial V/\partial M_{\mathrm{O}})_{T,P}$ given in Table IV. In accordance with Eq. (1), the electron-phonon contributions $(\partial E_{gx}/\partial M_{\mathrm{Zn}})_{T,V}$ and $(\partial E_{gx}/\partial M_{\mathrm{O}})_{T,V}$ are obtained by subtracting the volume related term $(D/V)\times(\partial V/\partial M)_{T,P}$ from $(\partial E_{gx}/\partial M)_{T,P}$.

Fitting the deduced low-temperature band gaps with Eq. (9) yields the unrenormalized band gaps for the static lattice as well as the coefficients C_{Zn}, C_{O}, shown in columns 2–4 of Table V, respectively. The last column of Table V displays the zero-point renormalizations in ZnO with natural isotopic composition, obtained using expression $-C_{\mathrm{Zn}}M_{\mathrm{Zn}}^{-1/2}-C_{\mathrm{O}}M_{\mathrm{O}}^{-1/2}$. The renormalization is the same, within experimental errors, for all three band gaps and the value determined for the excitonic gap A is in excellent agreement with (−164±9) meV obtained by Manjón *et al.*[18]

CONCLUSIONS

The present paper reports the isotopic mass dependence of the A, B, and C direct excitonic band gaps of ZnO at low temperatures, deduced from wavelength-modulated reflectivity measurements on isotopically engineered ZnO. The lineshape analysis of the reflectivity spectra based on the polariton model has allowed us to obtain the A, B, and C transverse exciton energies as functions of the isotopic masses of Zn and O. The dependence is analyzed in terms of zero-point renormalization of the band gap by electron-phonon interaction and the dependence of volume on isoto-

TABLE IV. Isotopic mass dependence of the A, B, and C excitonic band gaps of ZnO at 10 K.

Excitonic band gap	A	B	C
$(\partial E_{gx}/\partial M_{\mathrm{Zn}})_{T,P}$ (meV/amu)	0.35±0.09	0.27±0.14	0.40±0.12
$(D/V)(\partial V/\partial M_{\mathrm{Zn}})_{T,P}$ (meV/amu)	−0.032	−0.033	−0.036
$(\partial E_{gx}/\partial M_{\mathrm{Zn}})_{T,V}$ (meV/amu)	0.38±0.09	0.30±0.14	0.44±0.12
$(\partial E_{gx}/\partial M_{\mathrm{O}})_{T,P}$ (meV/amu)	3.24±0.21	3.36±0.20	3.27±0.31
$(D/V)(\partial V/\partial M_{\mathrm{O}})_{T,P}$ (meV/amu)	0.72	0.75	0.81
$(\partial E_{gx}/\partial M_{\mathrm{O}})_{T,V}$ (meV/amu)	2.52±0.21	2.61±0.20	2.46±0.31

TABLE V. The A, B, and C excitonic band gaps for static ZnO lattice and their zero-point renormalizations.

Excitonic band gap	E_{gx}^{∞} (eV)	C_{Zn} (eV amu$^{1/2}$)	C_{O} (eV amu$^{1/2}$)	$E_{gx}^{\infty}-E_{gx}(^{nat}\mathrm{Zn}^{nat}\mathrm{O})$ (eV)
A	3.531±0.010	−0.343±0.075	−0.449±0.018	0.154±0.014
B	3.526±0.009	−0.254±0.064	−0.454±0.016	0.145±0.012
C	3.590±0.011	−0.412±0.074	−0.471±0.018	0.169±0.014

pic mass, which are approximated for binary ZnO by a two-oscillator model involving a Zn-dominated and an O-dominated Einstein oscillator. Fitting the isotopic dependence of the A, B, and C excitonic band gaps to the simple analytical expression, predicted by the two-oscillator model, allows us to determine their values for the static lattice and corresponding zero-point renormalizations. All three band gaps experience the same amount of zero-point renormalization within the experimental errors.

Analysis of the two renormalization mechanisms shows that electron-phonon interaction accounts for ~80% of the total zero-point renormalization of the A, B, and C excitonic band gaps in ZnO. In addition, treatment of the dependence of volume on isotopic mass at zero temperature in the spirit of the two-oscillator model predicts an increase of volume with the mass of O and an anomalous decrease with the mass of Zn, subject to theoretical and experimental verification.

ACKNOWLEDGMENT

The authors at Purdue thank the National Science Foundation for support through Grants No. DMR-0102699 and No. DMR-0405082.

*Present address: Center for Bio/Molecular Science and Engineering, Naval Research Laboratory, Washington, DC 20375, USA.

[1] Isotopic Effects in Semiconductors, a special issue of Solid State Commun. **133** (2005).
[2] M. Cardona and M. L. W. Thewalt, Rev. Mod. Phys. **77**, 1173 (2005).
[3] T. R. Anthony, W. F. Banholzer, J. F. Fleischer, L. Wei, P. K. Kuo, R. L. Thomas, and R. W. Pryor, Phys. Rev. B **42**, 1104 (1990).
[4] L. Wei, P. K. Kuo, R. L. Thomas, T. R. Anthony, and W. F. Banholzer, Phys. Rev. Lett. **70**, 3764 (1993).
[5] F. Widulle, T. Ruf, M. Konuma, I. Silier, M. Cardona, W. Kriegseis, and V. I. Ozhogin, Solid State Commun. **118**, 1 (2001).
[6] A. T. Collins, S. C. Lawson, G. Davies, and H. Kanda, Phys. Rev. Lett. **65**, 891 (1990).
[7] G. Davies, E. C. Lightowlers, K. Itoh, W. L. Hansen, E. E. Haller, and V. Ozhogin, Semicond. Sci. Technol. **7**, 1271 (1992).
[8] C. Parks, A. K. Ramdas, S. Rodriguez, K. M. Itoh, and E. E. Haller, Phys. Rev. B **49**, 14244 (1994).
[9] P. Etchegoin, J. Weber, M. Cardona, W. L. Hansen, K. Itoh, and E. E. Haller, Solid State Commun. **83**, 843 (1992).
[10] D. Karaiskaj, M. L. W. Thewalt, T. Ruf, M. Cardona, and M. Konuma, Solid State Commun. **123**, 87 (2002).
[11] S. Tsoi, H. Alawadhi, X. Lu, J. W. Ager III, C. Y. Liao, H. Riemann, E. E. Haller, S. Rodriguez, and A. K. Ramdas, Phys. Rev. B **70**, 193201 (2004).
[12] See, for example, A. K. Ramdas, S. Rodriguez, S. Tsoi, and E. E. Haller, Solid State Commun. **133**, 709 (2005).
[13] See, T. A. Meyer, M. L. W. Thewalt, M. Cardona, and R. Lauck, Phys. Rev. B **69**, 115214 (2004), and references therein.
[14] A. Göbel, T. Ruf, M. Cardona, C. T. Lin, J. Wrzesinski, M. Steube, K. Reimann, J.-C. Merle, and M. Joucla, Phys. Rev. B **57**, 15183 (1998).
[15] J. Serrano, Ch. Schweitzer, C. T. Lin, K. Reimann, M. Cardona, and D. Fröhlich, Phys. Rev. B **65**, 125110 (2002).
[16] J. M. Zhang, T. Ruf, R. Lauck, and M. Cardona, Phys. Rev. B **57**, 9716 (1998).
[17] F. I. Kreingol'd and B. S. Kulinkin, Sov. Phys. Solid State **28**, 1781 (1986).
[18] F. J. Manjón, M. Mollar, M. A. Hernández-Fenollosa, B. Marí, R. Lauck, and M. Cardona, Solid State Commun. **128**, 35 (2003).
[19] J. Serrano, F. J. Manjon, A. H. Romero, F. Widulle, R. Lauck, and M. Cardona, Phys. Rev. Lett. **90**, 055510 (2003).
[20] S. Tsoi, Ph.D. thesis, Purdue University, 2005.
[21] A. Debernardi and M. Cardona, Phys. Rev. B **54**, 11305 (1996); see also N. Garro, A. Cantarero, M. Cardona, A. Göbel, T. Ruf, and K. Eberl, *ibid.* **54**, 4732 (1996).
[22] D. Olguin, M. Cardona, and A. Cantarero, Solid State Commun. **122**, 575 (2002).
[23] R. Pässler, J. Appl. Phys. **89**, 6235 (2001).
[24] M. Cardona, T. A. Meyer, and M. L. W. Thewalt, Phys. Rev. Lett. **92**, 196403 (2004).
[25] See, for example, A. Mang, K. Reimann, and St. Rübenacke, Solid State Commun. **94**, 251 (1995).
[26] W. Y. Liang and A. D. Yoffe, Phys. Rev. Lett. **20**, 59 (1968).
[27] M. Cardona, in *Solid State Physics*, Suppl. 11, edited by F. Seitz, D. Turnbull, and H. Ehrenreich (Academic Press, New York, 1969), p. 89.
[28] J. J. Hopfield and D. G. Thomas, Phys. Rev. **132**, 563 (1963).
[29] T. Skettrup and I. Balslev, Phys. Rev. B **3**, 1457 (1971).
[30] S. I. Pekar, Sov. Phys. Solid State **4**, 953 (1962).
[31] F. Evangelisti, A. Frova, and F. Patella, Phys. Rev. B **10**, 4253 (1974).
[32] J. J. Hopfield and D. G. Thomas, J. Phys. Chem. Solids **12**, 276 (1960).

[33] J. Lagois and K. Hümmer, Phys. Status Solidi B **72**, 393 (1975).
[34] J. Serrano, A. H. Romero, F. J. Manjón, R. Lauck, M. Cardona, and A. Rubio, Phys. Rev. B **69**, 094306 (2004).
[35] J. Emsley, *The Elements*, 2nd ed. (Clarendon Press, Oxford, 1991); Natural isotopic abundance: $^{nat}\mathrm{O} \equiv 99.762\,\%\,^{16}\mathrm{O} + 0.038\,\%\,^{17}\mathrm{O} + 0.200\,\%\,^{18}\mathrm{O} \equiv {}^{16}\mathrm{O}$, $^{nat}\mathrm{Zn} \equiv 48.6\,\%\,^{64}\mathrm{Zn} + 27.6\,\%\,^{66}\mathrm{Zn} + 4.1\,\%\,^{67}\mathrm{Zn} + 18.8\,\%\,^{68}\mathrm{Zn} + 0.6\,\%\,^{70}\mathrm{Zn} \equiv {}^{65.4}\mathrm{Zn}$.
[36] In the zinc-blende structure, these are the acoustic modes; in wurtzite, with two molecular units per primitive cell, these modes include acoustic and folded acoustic components, i.e., the three lowest optical phonon branches.